Low-Noise $YBa_2Cu_3O_7$ Nano-SQUIDs for Performing Magnetization-Reversal Measurements on Magnetic Nanoparticles

T. Schwarz,[1] R. Wölbing,[1] C. F. Reiche,[2] B. Müller,[1] M. J. Martínez-Pérez,[1] T. Mühl,[2] B. Büchner,[2] R. Kleiner,[1] and D. Koelle[1]

[1]*Physikalisches Institut-Experimentalphysik II and Center for Collective Quantum Phenomena in LISA$^+$, Universität Tübingen, Auf der Morgenstelle 14, D-72076 Tübingen, Germany*

[2]*Leibniz Institute for Solid State and Materials Research IFW Dresden, Helmholtzstrasse 20, 01069 Dresden, Germany*

(Received 1 October 2014; published 17 April 2015)

We fabricate $YBa_2Cu_3O_7$ (YBCO) direct-current nano- superconducting quantum-interference devices (nano-SQUIDs) based on grain-boundary Josephson junctions by focused-ion-beam patterning. Characterization of electric transport and noise properties at 4.2 K in a magnetically shielded environment yields a very small inductance L of a few pH for an optimized device geometry. This, in turn, results in very low values of flux noise $< 50\ n\Phi_0/Hz^{1/2}$ in the thermal white-noise limit, which yields spin sensitivities of a few $\mu_B/Hz^{1/2}$ (Φ_0 is the magnetic flux quantum, and μ_B is the Bohr magneton). We observe frequency-dependent excess noise up to 7 MHz, which can be eliminated only partially by bias reversal readout. This behavior indicates the presence of fluctuators of unknown origin, possibly related to defect-induced spins in the $SrTiO_3$ substrate. We demonstrate the potential of using YBCO nano-SQUIDs for the investigation of small spin systems, by placing a 39-nm-diameter Fe nanowire encapsulated in a carbon nanotube on top of a nonoptimized YBCO nano-SQUID and by measuring the magnetization reversal of the Fe nanowire via the change of magnetic flux coupled to the nano-SQUID. The measured flux signals upon magnetization reversal of the Fe nanowire are in very good agreement with estimated values, and the determined switching fields indicate magnetization reversal of the nanowire via curling mode.

DOI: 10.1103/PhysRevApplied.3.044011

I. INTRODUCTION

Small spin systems or magnetic nanoparticles (MNPs), like single-molecular magnets, nanowires, or nanotubes behave very differently from magnetic bulk material, which makes them very interesting, both for basic research and applications ranging from spintronics and spin-based quantum-information processing to industrial use of ferrofluidic devices and biomedical applications [1–7]. Because of their nanoscale size, MNPs have very small magnetic moments, which does not allow one to use standard magnetic characterization techniques for the investigation of their properties. In one approach, which has been pioneered by Wernsdorfer [8], MNPs are placed very close to miniaturized superconducting quantum-interference devices (SQUIDs), often referred to as micro-SQUIDs or nano-SQUIDs [9–25], and the magnetization reversal of MNPs is measured directly via the change of stray magnetic flux coupled to the micro-SQUIDs or nano-SQUIDs. Major challenges for this application are the development of SQUIDs (i) with ultralow flux noise, which can be achieved via the reduction of the inductance L of the SQUID loop and (ii) which can be operated in very large magnetic fields (up to the tesla range), without significant degradation of their noise performance.

The most common approach for the realization of direct-current (dc) nano-SQUIDs uses two constriction-type Josephson junctions (CJJs) intersecting the SQUID loop [11,12,14,16,23,26,27]. In this case, optimum coupling between a MNP and the nano-SQUID is achieved by placing the particle directly on top of one of the CJJs. The use of CJJs offers the possibility to operate the SQUIDs in strong magnetic fields. However, if conventional metallic superconductors such as Pb or Nb are used, high-field operation is limited by the upper critical field of typically 1 T for thin films [28]. Still, it has been demonstrated that by using ultrathin films, this limitation can be overcome [29]. However, with ultrathin films the SQUID inductance L is dominated by a large kinetic inductance contribution, which yields large flux noise. To date, the most successful approach is the SQUID on tip (SOT) [26]. With the so far smallest Pb SOT with 46-nm effective loop diameter and 15-nm film thickness, ultralow flux noise down to $50\ n\Phi_0/Hz^{1/2}$ at 4.2 K has been demonstrated [28] (Φ_0 is the magnetic flux quantum). The inductance for a slightly larger device (56-nm effective diameter) was estimated as $L = 5.8$ pH. The SOT technology is extremely powerful for high-resolution scanning SQUID microscopy and provides a spin sensitivity below $1\ \mu_B/Hz^{1/2}$ for certain intervals of applied magnetic field up to about 1 T (μ_B is the Bohr magneton) estimated for a pointlike MNP with 10 nm distance to the SOT. However, maintaining the optimum flux bias point in a variable

magnetic field is not possible; i.e., the flux noise and spin sensitivity strongly depend on the applied field, which makes such devices less interesting for the investigation of the magnetization reversal of MNPs.

An alternative approach is the use of $YBa_2Cu_3O_7$ (YBCO) dc nano-SQUIDs with grain-boundary Josephson junctions (GBJJs) for operation at temperature $T = 4.2$ K and below [30]. Magnetization reversal of a MNP can be detected by applying an in-plane magnetic field perpendicular to the grain boundary, i.e., without significant suppression of the GBJJ critical currents. The huge upper critical field of YBCO in the range of tens of teslas offers the possibility for operation in strong fields up to the tesla range, without using ultrathin films [31]. Hence, very low inductance devices with potentially ultralow flux noise can be realized.

Very recently, we performed an optimization study for the design of YBCO nano-SQUIDs [32]. This work is based on the calculation of the coupling factor ϕ_μ, i.e., the amount of magnetic flux coupled to the SQUID per magnetic moment of a pointlike MNP placed on top of a narrow constriction inserted into the SQUID loop. This additional constriction allows for the optimization of ϕ_μ (via constriction geometry) without affecting the junctions. In addition, we performed numerical simulations to calculate the SQUID inductance and root-mean-square (rms) spectral density of flux noise $S_{\Phi,w}^{1/2}$ in the thermal white-noise limit. This approach enabled us to predict the spin sensitivity in the thermal white-noise limit $S_{\mu,w}^{1/2} = S_{\Phi,w}^{1/2}/\phi_\mu$ for our devices as a function of all relevant device parameters. This optimization study predicts optimum performance for a YBCO film thickness $d \approx 120$ nm, which allows us to realize nano-SQUIDs with very small L of a few pH. For optimized devices, we predict $S_{\Phi,w}^{1/2}$ of several tens of $n\Phi_0/Hz^{1/2}$ and $\phi_\mu \sim 10$–$20\ n\Phi_0/\mu_B$ (for a MNP placed 10 nm above the YBCO film on top of the constriction) yielding a spin sensitivity $S_{\mu,w}^{1/2}$ of a few $\mu_B/Hz^{1/2}$.

Here, we report on the realization of optimized YBCO nano-SQUIDs based on GBJJs and on the experimental determination of their electric transport and noise properties in a magnetically shielded environment at $T = 4.2$ K. To demonstrate the suitability of our YBCO nano-SQUIDs for the detection of small spin systems, we present the measurement of the magnetization reversal (up to approximately 200 mT at $T = 4.2$ K) of an Fe nanowire with diameter $d_{Fe} = 39$ nm, which is positioned close the SQUID loop.

II. DEVICE FABRICATION AND EXPERIMENT SETUP

The fabrication of the devices is carried out according to Refs. [30,31]. A *c*-axis-oriented YBCO thin film of thickness d is grown epitaxially by pulsed laser deposition on a $SrTiO_3$ (STO) [001] bicrystal substrate with a 24° grain-boundary misorientation angle. An *in situ* evaporated Au layer of thickness d_{Au} serves as shunt resistance to provide nonhysteretic current-voltage characteristics (IVCs). SQUIDs with smallest line widths down to 50 nm are patterned by focused-ion-beam (FIB) milling with 30-keV Ga ions. The Au layer also minimizes Ga implantation into the YBCO film during FIB milling.

For characterization of the device properties, electric transport and noise measurements are performed in an electrically and magnetically shielded environment at $T = 4.2$ K, i.e., with the samples immersed into liquid He. By applying a modulation current I_{mod} across the constriction, the magnetic flux coupled to the SQUID can be modulated. This scheme allows flux biasing at the optimum working point and operation in a flux-locked loop (FLL) mode [33]. In FLL mode, a deviation from the voltage at the optimum working point (due to any flux signal), is amplified and then fed back via a feedback resistor as a feedback current through the constriction. The feedback current produces a feedback flux canceling the applied flux signal; i.e., the SQUID is always operated at its optimum working point, and the voltage across the feedback resistor (proportional to the flux signal) serves as the output signal. The readout in FLL mode is limited by the bandwidth of the feedback circuit. If the signals applied to the SQUID are small enough, one can also operate the SQUID in open-loop mode; i.e., the voltage across the SQUID is amplified without feedback, and the amplified voltage serves as the output signal. In this case, the readout is limited by the bandwidth of the voltage amplifier, which is typically larger than the FLL bandwidth. To determine the spectral density of flux noise S_Φ vs frequency f of the devices, we use a Magnicon SEL-1 SQUID electronics [34] in direct readout mode [35], which is either operated in open-loop mode (maximum bandwidth of approximately 7 MHz) or in FLL mode (maximum bandwidth of approximately 500–800 kHz). The SEL electronics allows for SQUID operation either with constant bias current (dc bias) or with a bias reversal readout scheme [maximum bias

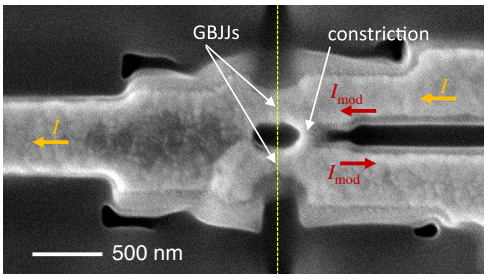

FIG. 1. SEM image of YBCO nano-SQUID-1. Vertical dashed line indicates position of the grain boundary intersecting the two SQUID arms. Horizontal arrows indicate paths for modulation current I_{mod} across the constriction and bias current I across the grain-boundary Josephson junctions.

TABLE I. Parameters of optimized SQUID-1 and -2 and of SQUID-3 used for measurements on Fe nanowire. Values for V_ϕ correspond to working points of noise measurements. Values in brackets for $S_{\Phi,w}^{1/2}$ and $S_{\mu,w}^{1/2}$ of SQUID-1 are based on the fitted noise spectrum. All devices have $d_{Au} = 70$ nm. SQUID-1 and -3 are measured at 4.2 K; SQUID-2 is measured at 5.3 K.

	d (nm)	l_c (nm)	l_J (nm)	w_c (nm)	w_{J1} (nm)	w_{J2} (nm)	β_L	L (pH)	I_c (μA)	R_N (Ω)	I_cR_N (mV)	V_Φ (mV/Φ_0)	$S_{\Phi,w}^{1/2}$ (nΦ_0/Hz$^{1/2}$)	ϕ_μ (nΦ_0/μ_B)	$S_{\mu,w}^{1/2}$ (μ_B/Hz$^{1/2}$)
SQUID-1	120	190	350	85	210	160	1.8	3.9	960	2.0	1.92	4.4	<50 (45)	13	<3.7 (3.4)
SQUID-2	120	230	370	100	180	230	0.94	6.3	311	2.5	0.78	1.7	<83	12	<6.7
SQUID-3	75	190	340	100	270	340	0.95	28	69	2.3	0.16	0.65	<1450	15	<98

reversal (BR) frequency $f_{BR} = 260$ kHz], to reduce $1/f$ noise caused by fluctuations of the critical currents $I_{0,1}$ and $I_{0,2}$ of the Josephson junctions 1 and 2, respectively [33].

Below we present the data of our best device, SQUID-1, with a $d = 120$-nm-thick YBCO film. Figure 1 shows a scanning electron microscope (SEM) image of SQUID-1. The loop size 350×190 nm^2 is given by the length l_J of the bridges straddling the grain boundary and by the length l_c of the constriction. SQUID-1 has junction widths $w_{J1} = 210$ nm and $w_{J2} = 160$ nm and a constriction width $w_c = 85$ nm. The parameters for SQUID-1 are summarized in Table I. For comparison, we also include parameters for a similar device, SQUID-2, which has the same YBCO film thickness, however, slightly larger inductance $L = 6.3$ pH, and about a factor of 2.5 smaller characteristic voltage $V_c \equiv I_cR_N$. I_c is the maximum critical current, and R_N is the asymptotic normal-state resistance of the SQUID. Details on electric transport and noise characteristics of SQUID-2 are presented in Sec. I of the Supplemental Material [36]. Those also include noise data taken from 6 to 65 K in a different setup with a temperature stability of approximately 1 mK [37]. Table I also includes parameters for SQUID-3, which is used for measurements on an Fe nanowire in a high-field setup, as discussed further below.

III. SQUID-1: ELECTRIC TRANSPORT AND NOISE

A. SQUID-1: Dc characteristics

Figure 2 shows the dc characteristics of SQUID-1. Figure 2(a) shows IVCs for $I_{mod} = 0$ and two values of I_{mod} corresponding to the maximum and minimum critical current. The IVCs are slightly hysteretic with maximum critical current $I_c = 960$ μA and $R_N = 2.0$ Ω, which yields $V_c = 1.92$ mV. The inset of Fig. 2(a) shows the modulation of the critical current $I_c(I_{mod})$. From the modulation period, we find for the magnetic flux Φ coupled to the SQUID by I_{mod} the mutual inductance $M = \Phi/I_{mod} = 0.44\Phi_0/\text{mA} = 0.91$ pH. We perform numerical simulations based on the resistively and capacitively shunted junction model to solve the coupled Langevin equations which include thermal fluctuations of the junction resistances [38]. From simulations of the $I_c(I_{mod})$ characteristics [cf. inset of Fig. 2(a)], we obtain for the screening parameter $\beta_L = 2I_0L/\Phi_0 = 1.8$ [with $I_0 = (I_{0,1} + I_{0,2})/2$], which yields a SQUID inductance $L = 3.9$ pH. We do find good agreement between the measured and simulated $I_c(I_{mod})$ characteristics if we include an inductance asymmetry $\alpha_L \equiv (L_2 - L_1)/(L_2 + L_1) = 0.20$ (L_1 and L_2

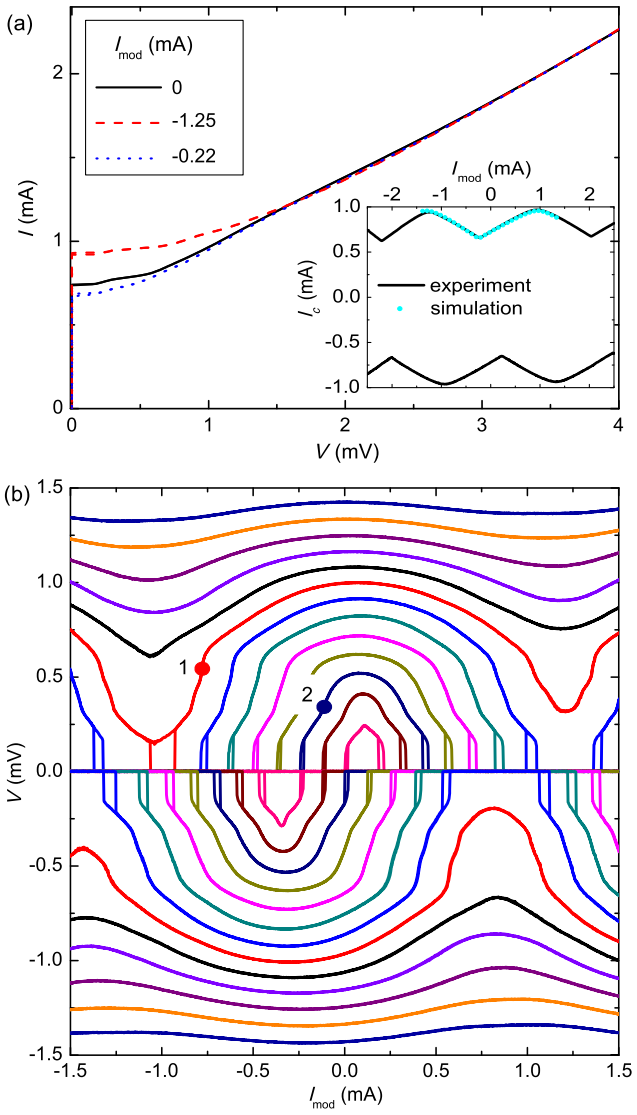

FIG. 2. SQUID-1 dc transport characteristics. (a) Measured IVCs for three different values of I_{mod}, including flux bias (I_{mod}) values which yield maximum and minimum critical current. Inset: Measured $I_c(I_{mod})$ for positive and negative current bias (solid lines) and numerical simulations (dots). (b) Measured $V(I_{mod})$ for bias currents $|I| = 0.64$–1.12 mA (in 40-μA steps). Points 1 and 2 are bias points with $V_\Phi = 12$ and 4.5 mV/Φ_0, respectively.

are the inductances of the two SQUID arms) and a critical current asymmetry $\alpha_I \equiv (I_{0,2} - I_{0,1})/(I_{0,2} + I_{0,1}) = 0.27$. These asymmetries are caused by asymmetric biasing of the SQUID and by asymmetries of the device itself.

$V(I_{\mathrm{mod}})$ is plotted in Fig. 2(b) for different bias currents. The transfer function, i.e., the maximum value of $\partial V/\partial\Phi$, in the nonhysteretic regime is $V_\Phi \approx 12\ \mathrm{mV}/\Phi_0$ [at $I = 0.92$ mA; cf. point 1 in Fig. 2(b)].

B. SQUID-1: Noise data

1. Open-loop mode

Figure 3(a) shows the rms spectral density of flux noise $S_\Phi^{1/2}(f)$ of SQUID-1 measured in open-loop mode to reach the highest possible bandwidth of the readout electronics. Because of the limitation in the maximum bias current of the readout electronics, noise spectra are taken at $I = 0.72$ mA with a transfer function $V_\Phi = 4.5\ \mathrm{mV}/\Phi_0$ [cf. point 2 in Fig. 2(b)]. Up to the cutoff frequency $f_{3\ \mathrm{dB}} = 7$ MHz, there is no white flux noise observable. Instead, the flux noise scales roughly as $S_\Phi \propto 1/f$, with $S_\Phi^{1/2} \approx 10\ \mu\Phi_0/\mathrm{Hz}^{1/2}$ at $f = 100$ Hz and $1\ \mu\Phi_0/\mathrm{Hz}^{1/2}$ at 10 kHz. This level of low-frequency excess noise is quite typical for YBCO GBJJ SQUIDs (also at $T = 77$ K) and has been ascribed to critical current fluctuations in the GBJJs [39]. However, due to the limitation by thermal white noise, typically between 1 and $10\ \mu\Phi_0/\mathrm{Hz}^{1/2}$ for low-noise YBCO SQUIDs, this f-dependent excess noise has not been observed so far up to the megahertz range. We note that for YBCO nano-SQUIDs implementing CJJs [27], a frequency-dependent $(1/f)$-like excess noise at $T = 8$ K of almost the same level as that for SQUID-1 was reported very recently and was also attributed to critical current fluctuations. For frequencies above 10 kHz, the flux noise of the YBCO nano-SQUID in Ref. [27] was limited by amplifier background noise.

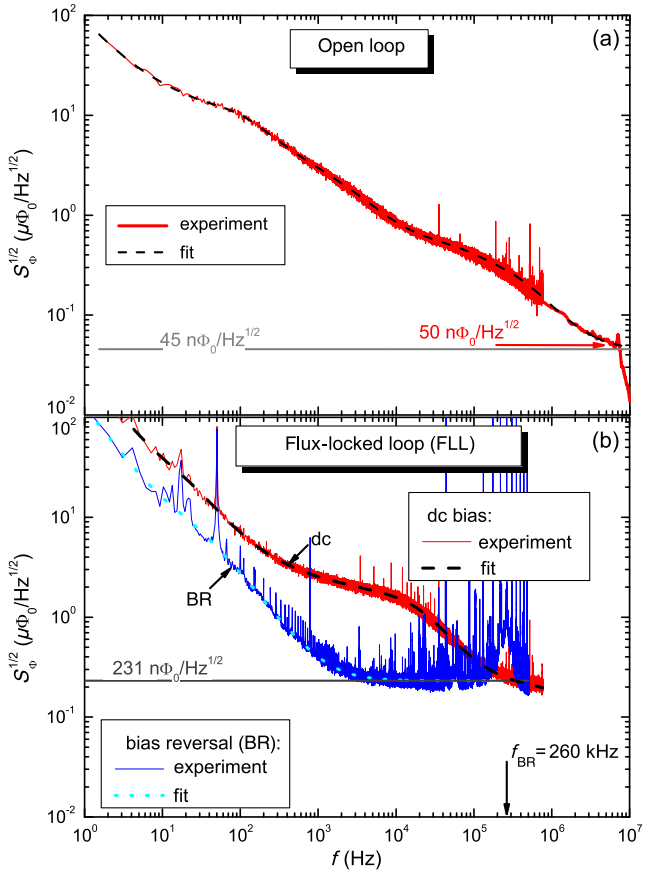

FIG. 3. Rms flux noise of SQUID-1. (a) Measured in open-loop mode at bias point 2 ($I = 0.72$ mA) in Fig. 2(b). Dashed line is a fit to the measured spectrum with white noise as indicated by the horizontal line. (b) Measured in FLL mode with dc bias and bias reversal ($|I| = 0.43$ mA, $V_\Phi = 4.4\ \mathrm{mV}/\Phi_0$). Vertical arrow indicates bias reversal frequency f_{BR}. Dashed and dotted lines are fits to the spectra; horizontal lines indicate fitted white noise.

For a more detailed analysis of the measured flux noise $S_\Phi(f)$, we apply an algorithm [40] to decompose the noise spectra into a sum of Lorentzians $F_i(f) = F_{0,i}/[1 + (f/f_{c,i})^2]$ plus a white-noise contribution F_w. The noise spectrum measured for SQUID-1 in open loop can be very well fitted by $F_{\mathrm{op}}(f) = F_{w,\mathrm{op}} + F_{s,\mathrm{op}} + \sum_{i=1}^{16} F_{\mathrm{op},i}(f)$, i.e., the superposition of a white-noise contribution with $F_{w,\mathrm{op}}^{1/2} = 45\ \mathrm{n}\Phi_0/\mathrm{Hz}^{1/2}$ plus a $1/f^2$ spectrum $F_{s,\mathrm{op}}$ (i.e., one or more Lorentzians with characteristic frequencies f_c well below 1 Hz) with $F_{s,\mathrm{op}}^{1/2}(1\ \mathrm{Hz}) = 84\ \mu\Phi_0/\mathrm{Hz}^{1/2}$ plus 16 Lorentzians, with $f_{c,i}$ ranging from 2.6 Hz to 2.6 MHz. For more details, see Sec. III of the Supplemental Material [36]. Hence, the decomposition of the spectrum into Lorentzians yields an estimate of the white rms flux noise $S_{\Phi,w}^{1/2} \approx 45\ \mathrm{n}\Phi_0/\mathrm{Hz}^{1/2}$ for SQUID-1. We note that this value for $S_{\Phi,w}^{1/2}$ is only a factor of 1.8 above the value, which we obtain from numerical simulations of the coupled Langevin equations [38] at $T = 4.2$ K for the parameters of SQUID-1.

Taking the measured flux noise at 7 MHz as an upper limit for $S_{\Phi,w}^{1/2}$, we still obtain a very low white rms flux noise, i.e., $S_{\Phi,w}^{1/2} < 50\ \mathrm{n}\Phi_0/\mathrm{Hz}^{1/2}$. This more conservative estimate for the white rms flux noise level is an improvement by more than an order of magnitude compared to our nonoptimized devices operated at 4.2 K and compared to the lowest value reported so far for a YBCO SQUID (at 8 K) very recently [27]. Furthermore, this value is the same as the lowest value reported for a Pb SOT operated at 4.2 K [28] and among the lowest flux noise levels ever achieved for a SQUID [9,41,42].

For the geometry of SQUID-1, we calculate [32] a coupling factor $\phi_\mu = 13.4\ \mathrm{n}\Phi_0/\mu_{\mathrm{B}}$ (10 nm above the YBCO film). With $S_{\Phi,w}^{1/2} < 50\ \mathrm{n}\Phi_0/\mathrm{Hz}^{1/2}$, we can determine an upper limit for the spin sensitivity (white-noise limit) of $S_{\mu,w}^{1/2} < 3.7\ \mu_B/\mathrm{Hz}^{1/2}$. If we take the fitted white

flux noise of 45 $n\Phi_0/Hz^{1/2}$, we obtain $S_{\mu,w}^{1/2} = 3.4\,\mu_B/Hz^{1/2}$. Hence, the achieved performance matches very well the predictions of our recent optimization study [32].

2. FLL mode: Dc bias vs bias reversal

Although the achieved low level of white flux noise for SQUID-1 is encouraging, one certainly will like to extend such a low-noise performance down to much lower frequencies. Therefore, we also perform noise measurements in FLL mode (with approximately 700-kHz bandwidth) and compare measurements with dc bias and bias reversal (with $f_{BR} = 260$ kHz). We note that the measurements in FLL mode are performed within a different cooling cycle, after SQUID-1 already shows a slight degradation in I_c [43]. Still, we are able to find a working point (at $|I| = 0.43$ mA) which yields almost the same transfer function, 4.4 mV/Φ_0, as for the measurement before degradation in open-loop mode.

Figure 3(b) shows rms flux noise spectra taken with dc bias and bias reversal. Comparing first the FLL dc bias measurement with the open-loop data, we note that the noise levels at f_{BR} coincide. For $f < f_{BR}$, the noise levels of the open-loop and FLL dc bias data are similar; however, the shape of the spectra differ, which we attribute to the above-mentioned degradation and variations between different cooling cycles. The dashed line in Fig. 3(b) is a fit to the measured spectral density of flux noise by $F_{dc}(f) = F_{w,dc} + \sum_{i=1}^{15} F_{dc,i}(f)$, i.e., the superposition of 15 Lorentzians, with $f_{c,i}$ ranging from 0.8 Hz to 6.8 MHz, plus a white-noise contribution $F_{w,dc}^{1/2} = 41\ n\Phi_0/Hz^{1/2}$, which we fix to a value similar to the white-noise level determined for the open-loop measurement. For more details, see Sec. III of the Supplemental Material [36].

Applying bias reversal, one expects a suppression of the contributions due to in-phase and out-of-phase critical current fluctuations of the GBJJs [39]. If the f-dependent excess noise below f_{BR} arises solely from I_0 fluctuations, one expects in bias reversal mode a frequency-independent noise for frequencies below the peak at f_{BR}, at a level which is given by the noise measured at f_{BR} in dc bias mode. This behavior can be observed for frequencies down to a few kilohertz, with an f-independent noise $F_{w,BR}^{1/2} = 231\ n\Phi_0/Hz^{1/2}$. For lower frequencies, however, we still find a strong f-dependent excess noise in bias reversal mode, which, hence cannot be attributed to I_0 fluctuations.

The spectral density of flux noise measured in bias reversal mode can be well approximated [cf. dotted line in Fig. 3(b)] by $F_{BR}(f) = F_{w,BR} + F_{s,BR} + \sum_{i=1}^{6} F_{BR,i}(f)$, with $F_{s,BR}^{1/2}(1\ Hz) = 128\ \mu\Phi_0/Hz^{1/2}$ and $f_{c,i}$ of the six Lorentzians ranging from 21 Hz to 5 kHz. For more details, see Sec. III of the Supplemental Material [36].

Obviously, below a few kilohertz, the low-frequency excess noise is dominated by slow fluctuators, which cannot be attributed to I_0 fluctuations. For different working points (I and I_{mod}) and also for other devices, the observation of low-f excess noise in bias reversal mode is reproducible [cf. flux noise data of SQUID-2 (from $T = 6$ K up to 65 K) and of SQUID-3 (at $T = 4.2$ K) in Secs. I and II, respectively, of the Supplemental Material [36]].

Considering the narrow linewidths of the SQUID structures, we estimate a threshold field for trapping of Abrikosov vortices [44] to be well above 1 mT. Since the measurements are performed in a magnetically shielded environment well below 100 nT, the presence of Abrikosov vortices as the source of the observed low-f fluctuators is very unlikely.

Low-frequency excess noise, which neither arises from I_0 nor from vortex fluctuations, has been reported during the last decades for SQUIDs based on conventional superconductors like Nb, Pb, PbIn, and Al, in particular, at temperatures well below 1 K [45]. This issue has recently been revived due to the increasing interest in the development of flux qubits and SQUIDs for ultra-low-temperature applications [46]. Various models have been suggested to describe the origin of such low-f excess noise, e.g., based on the coupling of magnetic moments associated with trapped electrons [47] or surface states [48,49], although the microscopic nature of defects as sources of excess "spin noise" still remains unclear.

For YBCO SQUIDs, excess low-f spin noise has not been addressed so far. However, it seems quite likely that defects are also a source of magnetic fluctuators in SQUIDs based on cuprates or any other oxide superconductors. Such defects can be present either in the thin-film SQUID structures themselves or in the substrates onto which the thin films are grown or at the interface between the thin film and the substrate.

The emergence and modification of magnetism at interfaces and surfaces of oxides, which are diamagnetic in the bulk, is currently an intensive field of research [50–52]. For STO, oxygen-vacancy-induced magnetism has been predicted [53], and experimental studies suggest ferromagnetic ordering up to room temperature [54], e.g., for defects induced by ion irradiation of single crystalline STO [55]. Furthermore, defect-induced magnetism in oxide grain boundaries and related defects have been suggested to be the intrinsic origin of ferromagnetism in oxides [56].

Obviously, further investigations on the impact and nature of such defects in our devices are needed and will be the subject of further studies. Such studies will include detailed noise measurements (dc vs bias reversal, variable flux bias, temperature, and magnetic field) to characterize and understand the f-dependent noise sources and, hopefully, eliminate them. Furthermore, readout with bias reversal at higher frequency up to the megahertz range in FLL mode has to be implemented in order to maintain the achieved ultralow white flux noise level down to lower frequencies. And finally, for applications of our nano-SQUIDs, it will be important to avoid

degradation in time, which shall be achieved by adding a suitable passivation layer, however, without introducing f-dependent excess noise.

IV. SQUID-3: MAGNETIZATION REVERSAL OF FE NANOWIRE

As a proof of principle, we demonstrate nano-SQUID measurements on the magnetization reversal of an Fe nanowire which is encapsulated in a carbon nanotube (CNT) [57]. Such iron-filled CNTs (Fe CNTs) are of fundamental interest with respect to studies on nanomagnetism. Furthermore, they are attractive for various applications, e.g., as tips in magnetic-force microscopy [58,59]. The Fe nanowire, which contains mainly single crystalline (ferromagnetic) α-Fe, has a diameter $d_{\mathrm{Fe}} = 39$ nm and length $l_{\mathrm{Fe}} = 13.8$ μm. The CNT has a diameter of approximately 130 nm. We note that this section is not directly related to the previous section in a sense to demonstrate the ultimate sensitivity of our devices on a magnetic nanoparticle with the smallest yet still detectable signals and operation in the strongest possible magnetic fields. Rather, we want to show an example of the feasibility of using our YBCO nano-SQUIDs for practical applications. As shown within this section, we can demonstrate signal-to-noise ratios which are clearly superior to micro-Hall measurements on similar nanowires.

The Fe CNT is positioned by a Kleindiek three-axis manipulator inside a FIB SEM combination onto SQUID-3, such that the distance between the left end of the Fe nanowire and the SQUID loop is approximately 300 nm (cf. Fig. 4). We note that for optimum coupling of the stray field of the Fe nanowire into the SQUID, it is preferable to place the end of the Fe nanowire close to the edge of the SQUID loop opposite the constriction. At this location, the coupling factor is slightly smaller than directly on top of the constriction; however, it does not fall off very rapidly upon moving farther away from the loop, as it is the case near the constriction [31]. The Fe nanowire axis (its easy axis) is aligned as close as possible with the substrate plane (x-y plane), with an inclination angle $\theta \approx 4°$ and perpendicular to the grain boundary, which is oriented along the y axis. The inclination of the Fe wire axis with respect to the x axis is $<1°$. The vertical distance (along the z axis) between the nanowire axis (at its left end) and the surface of the YBCO film is approximately 300 nm.

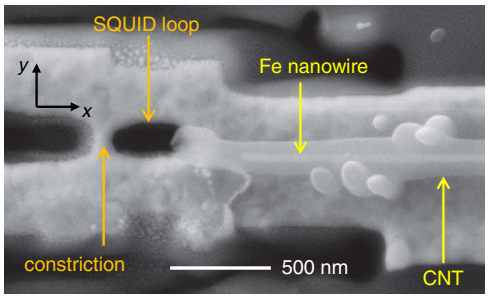

FIG. 4. SEM image of SQUID-3 with an Fe-wire-filled carbon nanotube positioned close to the SQUID loop.

The measurements on the Fe nanowire are performed with the nonoptimized SQUID-3. This device has a significantly larger inductance (due to its smaller film thickness) and much smaller characteristic voltage, resulting in a much smaller transfer function $V_\Phi = 0.65$ mV/Φ_0, as compared to SQUID-1 and -2. Magnetization-reversal measurements on the Fe CNT are performed with SQUID-3 operated in FLL dc bias mode up to $f = 190$ kHz. At this frequency, the noise is limited by the readout electronics, which yields for SQUID-3 an upper limit of the white rms flux noise $S_{\Phi,w}^{1/2} \leq 1.45\ \mu\Phi_0/\mathrm{Hz}^{1/2}$. Below approximately 40 kHz, SQUID-3 shows f-dependent excess noise with $S_\Phi^{1/2} \approx 8\ \mu\Phi_0/\mathrm{Hz}^{1/2}$ at $f = 100$ Hz and $S_\Phi^{1/2} \approx 20\ \mu\Phi_0/\mathrm{Hz}^{1/2}$ at $f = 10$ Hz, with an approximately $1/f^2$ increase of S_Φ below 10 Hz. Some experimentally determined parameters of SQUID-3 are listed in Table I. Details on low-field electric transport and noise characteristics of SQUID-3 are presented in Sec. II of the Supplemental Material [36].

For magnetization-reversal measurements of the Fe nanowire on top of SQUID-3, the sample is mounted in a high-field setup, which allows us to apply magnetic fields up to $\mu_0 H = 7$ T [31]. To minimize coupling of the external magnetic field H into the SQUID, the SQUID loop (in the x-y plane) is aligned parallel to the field. To minimize coupling of the external field into the GBJJs, the grain boundary (along the y axis) is aligned perpendicular to the applied field. The alignment of the SQUID with respect to the applied field direction is performed by an Attocube system including two goniometers with perpendicular tilt axes and one rotator. In this configuration, the external field H is applied along the x axis (cf. Fig. 4), and the angle between H and the Fe nanowire axis is given by θ.

Figure 5 shows the flux signal $\Phi(H)$ detected by SQUID-3, while sweeping H, at a rate $\mu_0 \partial H/\partial t \approx 1$ mT/s. At the fields $\pm\mu_0 H_n = \pm 101$ mT, abrupt changes by $\Delta\Phi \approx 150$ mΦ_0 clearly indicate magnetization reversal of the Fe nanowire. The shape of the $\Phi(H)$ curve indicates magnetization reversal of a single-domain particle. The slope of the curve in the interval $-H_n \leq H \leq H_n$ depends strongly on the alignment of the SQUID with respect to the applied field. Hence, this slope can be attributed, at least partially, to the coupling of the external field to the SQUID loop. The hysteresis in the signals for $|H| \gtrsim 100$ mT is typically observed also for our SQUIDs measured in the high-field setup without MNPs coupled to them. Hence, this hysteresis is attributed to a spurious magnetization signal from our setup or from the above-mentioned magnetic defects close to the nano-SQUID, rather than being generated by the nanowire.

In order to convert from magnetic flux detected by the SQUID to magnetization of the Fe nanowire, we follow the

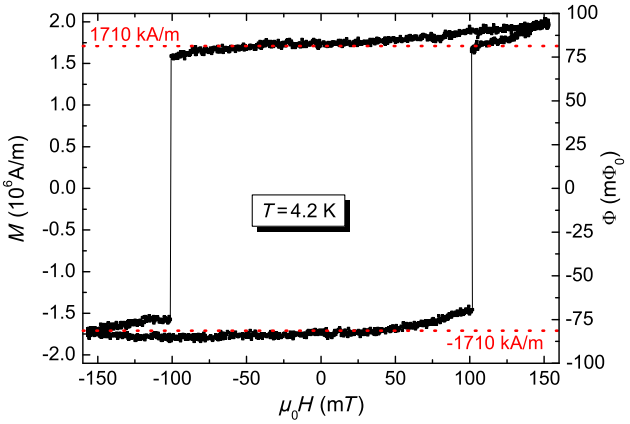

FIG. 5. Hysteresis loop $\Phi(H)$ of the Fe nanowire detected with SQUID-3 (operated in FLL dc bias mode with cutoff frequency approximately 190 kHz, at optimum working point with $V_\Phi = 0.65\ \mathrm{mV}/\Phi_0$). Switching of the magnetization occurs at $\pm\mu_0 H_n = \pm 101$ mT. The residual field $\mu_0 H_{\mathrm{res}} = 4.0$ mT is subtracted. Left axis indicates corresponding magnetization $M = \Phi/\phi_M$; the dashed lines indicate the literature's value of the saturation magnetization $\pm M_s$.

approach described in Ref. [60]. We numerically calculate the coupling factor $\phi_\mu(\hat{e}_\mu, \vec{r}_p)$ for a pointlike MNP with orientation $\hat{e}_\mu$ of its magnetic moment at position $\vec{r}_p$ in the 3D space above the SQUID [32]. These simulations take explicitly into account the geometry of SQUID-3 and are based on London theory [61]. We then assume that the Fe nanowire is in its fully saturated state, with saturation magnetization M_s, with all moments oriented along the wire axis. The corresponding saturation flux coupled to the SQUID is denoted as Φ_s. The ratio Φ_s/M_s is obtained by integration of the coupling factor ϕ_μ over the volume V_{Fe} of the Fe wire, at its given position, determined from SEM images. This integration yields

$$\phi_M \equiv \frac{\Phi_s}{M_s} = \int_{V_{\mathrm{Fe}}} \phi_\mu(\vec{r}_p)dV = 47.6\frac{\mathrm{n}\Phi_0}{\mathrm{Am}^{-1}}. \qquad (1)$$

From this result, we calculate $\Phi_s = M_s\phi_M = 81.4\ \mathrm{m}\Phi_0$, with $M_s = 1710$ kA/m taken from the literature [62]. The comparison with the measured flux signals $\pm 82.5\ \mathrm{m}\Phi_0$ at $H = 0$ shows very good agreement. The left axis in Fig. 5 shows the magnetization axis scaled as $M = \Phi/\phi_M$ with the horizontal dotted lines indicating the literature's value $M_s = \pm 1710$ kA/m. Hence, the measured flux signals are also in quantitative agreement with the assumption that the Fe nanowire switches to a fully saturated single-domain state.

In Ref. [58], it was shown for a similar Fe CNT that the nucleation field H_n changes with θ in a way which is typical for nucleation of magnetization reversal via the curling mode [63] in ferromagnetic nanowires as opposed to uniform rotation of the magnetic moments in small enough MNPs as described by the Stoner-Wolfarth model [64]. For switching via curling mode, one obtains for $\theta = 0$ the simple relation $H_n = M_s a/2$, with a negligible increase well below 1% with $\theta = 4°$ [65]. Here, $a = 1.08(2\lambda_{\mathrm{ex}}/d_{\mathrm{Fe}})^2$, with the exchange length $\lambda_{\mathrm{ex}} = \sqrt{4\pi A/(\mu_0 M_s^2)}$ and the exchange constant A [62]. For $d_{\mathrm{Fe}} = 39$ nm and with $\lambda_{\mathrm{ex}} = 5.8$ nm [62], we obtain $a = 0.0955$, and with $M_s = 1710$ kA/m, we obtain an estimate of the nucleation field $H_n = 103$ mT, which is in very good agreement with the experimentally observed value.

Finally, we note that the SQUID measurement yields a noise amplitude of approximately 1 $\mathrm{m}\Phi_0$, which is 2 orders of magnitude smaller than the detected signal upon magnetization reversal. For comparison, measurements on a similar Fe nanowire by micro-Hall magnetometry yield a noise amplitude which was about 1 order of magnitude below the switching signal [58]. Hence, the use of our nano-SQUID improves the signal-to-noise ratio by about 1 order of magnitude.

V. CONCLUSIONS

In conclusion, we fabricate and investigate optimized YBCO nano-SQUIDs based on grain-boundary Josephson junctions. For our best device, an upper limit for the white flux noise level $S_\Phi^{1/2} < 50\ \mathrm{n}\Phi_0/\mathrm{Hz}^{1/2}$ in magnetically shielded environment can be determined, which corresponds to a spin sensitivity $S_\mu^{1/2} \equiv S_\Phi^{1/2}/\phi_\mu = 3.7\ \mu_B/\mathrm{Hz}^{1/2}$ for a magnetic nanoparticle located 10 nm above the constriction in the SQUID loop. Here, the coupling factor ϕ_μ is determined by numerical simulations based on London theory, which takes the device geometry into account. An obvious drawback of YBCO grain-boundary junction nano-SQUIDs is the frequency-dependent excess noise, which extends up to the megahertz range for optimized devices with ultralow flux noise in the white-noise limit. To eliminate $1/f$ noise, a bias reversal scheme is applied, which reduces only the frequency-dependent excess noise partially. Hence, in addition to critical current fluctuations, spin noise which is possibly due to fluctuations of defect-induced magnetic moments in the $SrTiO_3$ substrate is a major issue, which has to be studied in more detail for further improvement of the nano-SQUID performance at low frequencies. Nevertheless, we demonstrate the suitability of the YBCO nano-SQUIDs as detectors for magnetic nanoparticles in moderate magnetic fields by measuring the magnetization reversal of an iron nanowire that is placed close to the SQUID loop. Switching of the magnetization is detected at $\mu_0 H \approx \pm 100$ mT, which is in very good agreement with nucleation of magnetization reversal via curling mode.

ACKNOWLEDGMENTS

T. S. acknowledges support by the Carl-Zeiss-Stiftung. M. J. M.-P. acknowledges support by the Alexander von

Humboldt Foundation. We gratefully acknowledge fruitful discussions with D. Drung (Physikalisch-Technische Bundesanstalt Berlin) and technical support by M. Turad and R. Löffler [instrument scientists of the core facility Center for Light-Matter Interaction, Sensors & Analytics (LISA$^+$)]. This work is supported by the Nachwuchswissenschaftlerprogramm of the Universität Tübingen, by the Deutsche Forschungsgemeinschaft (DFG) via Projects No. KO 1303/13-1, No. MU 1794/3-2, and No. SFB/TRR 21 C2 and by the EU-FP6-COST Action MP1201.

[1] *Molecular Magnets: Physics and Applications*, edited by Juan Bartolomé, Fernando Luis, and Julio F. Fernández (Springer, Heidelberg, 2014).

[2] Lapo Bogani and Wolfgang Wernsdorfer, Molecular spintronics using single-molecule magnets, Nat. Mater. **7**, 179 (2008).

[3] Michael N. Leuenberger and Daniel Loss, Quantum computing in molecular magnets, Nature (London) **410**, 789 (2001).

[4] S. Odenbach, Ferrofluids and their applications, MRS Bull. **38**, 921 (2013).

[5] Andreas Jordan, Regina Scholz, Peter Wust, Horst Fähling, and Roland Felix, Magnetic fluid hyperthermia (MFH): Cancer treatment with AC magnetic field induced excitation of biocompatible superparamagnetic nanoparticles, J. Magn. Magn. Mater. **201**, 413 (1999).

[6] R. C. Semelka and T. K. G. Helmberger, State of the art: Contrast agents for MR imaging of the liver, Radiology **218**, 27 (2001).

[7] R. Klingeler, S. Hampel, and B. Büchner, Carbon nanotube based biomedical agents for heating, temperature sensoring and drug delivery, International Journal of Hyperthermia **24**, 496 (2008).

[8] W. Wernsdorfer, Classical and quantum magnetization reversal studied in nanometersized particles and clusters, Adv. Chem. Phys. **118**, 99 (2001).

[9] D. D. Awschalom, J. R. Rozen, M. B. Ketchen, W. J. Gallagher, A. W. Kleinsasser, R. L. Sandstrom, and B. Bumble, Low-noise modular microsusceptometer using nearly quantum limited dc SQUIDs, Appl. Phys. Lett. **53**, 2108 (1988).

[10] M. Ketchen, D. Awschalom, W. Gallagher, A. Kleinsasser, R. Sandstrom, J. Rozen, and B. Bumble, Design, fabrication, and performance of integrated miniature SQUID susceptometers, IEEE Trans. Magn. **25**, 1212 (1989).

[11] K. Hasselbach, D. Mailly, and J. R. Kirtley, Micro-superconducting quantum interference device characteristic, J. Appl. Phys. **91**, 4432 (2002).

[12] S. K. H. Lam and D. L. Tilbrook, Development of a niobium nanosuperconducting quantum interference device for the detection of small spin populations, Appl. Phys. Lett. **82**, 1078 (2003).

[13] J.-P. Cleuziou, W. Wernsdorfer, V. Bouchiat, T. Ondarçuhu, and M. Monthioux, Carbon nanotube superconducting quantum interference device, Nat. Nanotechnol. **1**, 53 (2006).

[14] Aico G. P. Troeman, Hendrie Derking, Bert Borger, Johannes Pleikies, Dick Veldhuis, and Hans Hilgenkamp, NanoSQUIDs based on niobium constrictions, Nano Lett. **7**, 2152 (2007).

[15] Nicholas C. Koshnick, Martin E. Huber, Julie A. Bert, Clifford W. Hicks, Jeff Large, Hal Edwards, and Kathryn A. Moler, A terraced scanning super conducting quantum interference device susceptometer with submicron pickup loops, Appl. Phys. Lett. **93**, 243101 (2008).

[16] L. Hao, J. C. Macfarlane, J. C. Gallop, D. Cox, J. Beyer, D. Drung, and T. Schurig, Measurement and noise performance of nano-superconducting-quantum-interference devices fabricated by focused ion beam, Appl. Phys. Lett. **92**, 192507 (2008).

[17] C. P. Foley and H. Hilgenkamp, Why NanoSQUIDs are important: An introduction to the focus issue, Supercond. Sci. Technol. **22**, 064001 (2009).

[18] V. Bouchiat, Detection of magnetic moments using a nano-squid: Limits of resolution and sensitivity in near-field squid magnetometry, Supercond. Sci. Technol. **22**, 064002 (2009).

[19] W. Wernsdorfer, From micro- to nano-SQUIDs: Applications to nanomagnetism, Supercond. Sci. Technol. **22**, 064013 (2009).

[20] Francesco Giazotto, Joonas T. Peltonen, Matthias Meschke, and Jukka P. Pekola, Superconducting quantum interference proximity transistor, Nat. Phys. **6**, 254 (2010).

[21] M. J. Martínez-Pérez, E. Bellido, R. de Miguel, J. Sesé, A. Lostao, C. Gómez-Moreno, D. Drung, T. Schurig, D. Ruiz-Molina, and F. Luis, Alternating current magnetic susceptibility of a molecular magnet submonolayer directly patterned onto a micro superconducting quantum interference device, Appl. Phys. Lett. **99**, 032504 (2011).

[22] E. J. Romans, S. Rozhko, L. Young, A. Blois, L. Hao, D. Cox, and J. C. Gallop, Noise performance of niobium nano-SQUIDs in applied magnetic fields, IEEE Trans. Appl. Supercond. **21**, 404 (2011).

[23] R. Russo, C. Granata, E. Esposito, D. Peddis, C. Cannas, and A. Vettoliere, Nanoparticle magnetization measurements by a high sensitive nano-superconducting quantum interference device, Appl. Phys. Lett. **101**, 122601 (2012).

[24] Carmine Granata, Antonio Vettoliere, Roberto Russo, Matteo Fretto, Natascia De Leo, and Vincenzo Lacquaniti, Three-dimensional spin nanosensor based on reliable tunnel Josephson nano-junctions for nanomagnetism investigations, Appl. Phys. Lett. **103**, 102602 (2013).

[25] D. Drung, J.-H. Storm, F. Ruede, A. Kirste, M. Regin, T. Schurig, A. M. Repollés, J. Sesé, and F. Luis, Thin-film microsusceptometer with integrated nanoloop, IEEE Trans. Appl. Supercond. **24**, 1600206 (2014).

[26] Amit Finkler, Yehonathan Segev, Yuri Myasoedov, Michael L. Rappaport, Lior Ne'eman, Denis Vasyukov, Eli Zeldov, Martin E. Huber, Jens Martin, and Amir Yacoby, Self-aligned nanoscale SQUID on a tip, Nano Lett. **10**, 1046 (2010).

[27] R. Arpaia, M. Arzeo, S. Nawaz, S. Charpentier, F. Lombardi, and T. Bauch, Ultra low noise $YBa_2Cu_3O_{7-\delta}$

nano superconducting quantum interference devices implementing nanowires, Appl. Phys. Lett. **104**, 072603 (2014).
[28] Denis Vasyukov, Yonathan Anahory, Lior Embon, Dorri Halbertal, Jo Cuppens, Lior Ne'eman, Amit Finkler, Yehonathan Segev, Yuri Myasoedov, Michael L. Rappaport, Martin E. Huber, and Eli Zeldov, A scanning superconducting quantum interference device with single electron spin sensitivity, Nat. Nanotechnol. **8**, 639 (2013).
[29] Lei Chen, Wolfgang Wernsdorfer, Christos Lampropoulos, George Christou, and Irinel Chiorescu, On-chip SQUID measurements in the presence of high magnetic fields, Nanotechnology **21**, 405504 (2010).
[30] J. Nagel, K. B. Konovalenko, M. Kemmler, M. Turad, R. Werner, E. Kleisz, S. Menzel, R. Klingeler, B. Büchner, R. Kleiner, and D. Koelle, Resistively shunted $YBa_2Cu_3O_7$ grain boundary junctions and low-noise SQUIDs patterned by a focused ion beam down to 80 nm linewidth, Supercond. Sci. Technol. **24**, 015015 (2011).
[31] T. Schwarz, J. Nagel, R. Wölbing, M. Kemmler, R. Kleiner, and D. Koelle, Low-noise nano superconducting quantum interference device operating in tesla magnetic fields, ACS Nano **7**, 844 (2013).
[32] R. Wölbing, T. Schwarz, B. Müller, J. Nagel, M. Kemmler, R. Kleiner, and D. Koelle, Optimizing the spin sensitivity of grain boundary junction nanoSQUIDs–Towards detection of small spin systems with single-spin resolution, Supercond. Sci. Technol. **27**, 125007 (2014).
[33] D. Drung and M. Mück, in *The SQUID Handbook*, edited by John Clarke and Alex I. Braginski, Fundamentals and Technology of SQUIDs and SQUID Systems Vol. 1 (Wiley-VCH, Weinheim, 2004), Chap. 4, pp. 127–170.
[34] SQUID electronics SEL-1, http://www.magnicon.com.
[35] D. Drung, High-t_c and low-t_c dc SQUID electronics, Supercond. Sci. Technol. **16**, 1320 (2003).
[36] See the Supplemental Material at http://link.aps.org/supplemental/10.1103/PhysRevApplied.3.044011 for additional data and analysis of SQUID-1, -2 and -3.
[37] M. Kemmler, D. Bothner, K. Ilin, M. Siegel, R. Kleiner, and D. Koelle, Suppression of dissipation in Nb thin films with triangular antidot arrays by random removal of pinning sites, Phys. Rev. B **79**, 184509 (2009).
[38] B. Chesca, R. Kleiner, and D. Koelle, in *The SQUID Handbook*, edited by John Clarke and Alex I. Braginski, Fundamentals and Technology of SQUIDs and SQUID systems Vol. 1 (Wiley-VCH, Weinheim, 2004), Chap. 2, pp. 29–92.
[39] D. Koelle, R. Kleiner, F. Ludwig, E. Dantsker, and John Clarke, High-transition-temperature superconducting quantum interference devices, Rev. Mod. Phys. **71**, 631 (1999).
[40] E. Sassier, R. Kleiner, and D. Koelle, A spectroscopic method for excess-noise spectrum analysis (unpublished).
[41] D. J. Van Harlingen, Roger H. Koch, and John Clarke, Superconducting quantum interference device with very low magnetic flux noise energy, Appl. Phys. Lett. **41**, 197 (1982).
[42] E. M. Levenson-Falk, R. Vijay, N. Antler, and I. Siddiqi, A dispersive nanoSQUID magnetometer for ultra-low noise, high bandwidth flux detection, Supercond. Sci. Technol. **26**, 055015 (2013).
[43] From measurements on a similar device, we find an almost linear decrease in I_c with time, with an approximately 20% reduction in I_c after 40 days. This rate of degradation is typical for most of our devices. A possible explanation of this effect is outdiffusion of oxygen from the submicron GBJJs along the *a-b* plane of the YBCO thin film.
[44] G. Stan, S. B. Field, and J. M. Martinis, Critical Field for Complete Vortex Expulsion from Narrow Superconducting Strips, Phys. Rev. Lett. **92**, 097003 (2004).
[45] Frederick C. Wellstood, Cristian Urbina, and John Clarke, Low-frequency noise in dc superconducting quantum interference devices below 1 K, Appl. Phys. Lett. **50**, 772 (1987).
[46] D. Drung, J. Beyer, J.-H. Storm, M. Peters, and T. Schurig, Investigation of low-frequency excess flux noise in dc SQUIDs at mK temperatures, IEEE Trans. Appl. Supercond. **21**, 340 (2011).
[47] Roger H. Koch, David P. DiVincenzo, and John Clarke, Model for $1/f$ Flux Noise in SQUIDs and Qubits, Phys. Rev. Lett. **98**, 267003 (2007).
[48] Rogerio de Sousa, Dangling-bond spin relaxation and magnetic $1/f$ noise from the amorphous-semiconductor/oxide interface: Theory, Phys. Rev. B **76**, 245306 (2007).
[49] S. Sendelbach, D. Hover, A. Kittel, M. Mück, John M. Martinis, and R. McDermott, Magnetism in SQUIDs at Millikelvin Temperatures, Phys. Rev. Lett. **100**, 227006 (2008).
[50] M. Venkatesan, C. B. Fitzgerald, and J. M. D. Coey, Thin films: Unexpected magnetism in a dielectric oxide, Nature (London) **430**, 630 (2004).
[51] N. Pavlenko, T. Kopp, E. Y. Tsymbal, J. Mannhart, and G. A. Sawatzky, Oxygen vacancies at titanate interfaces: Two-dimensional magnetism and orbital reconstruction, Phys. Rev. B **86**, 064431 (2012).
[52] J. M. D. Coey, Ariando, and W. E. Pickett, Magnetism at the edge: New phenomena at oxide interfaces, MRS Bull. **38**, 1040 (2013).
[53] I. R. Shein and A. L. Ivanosvkii, First principle prediction of vacancy-induced magnetism in non-magnetic Perovskite $SrTiO_3$, Phys. Lett. A **371**, 155 (2007).
[54] M. Khalid, A. Setzer, M. Ziese, P. Esquinazi, D. Spemann, A. Pöppl, and E. Goering, Ubiquity of ferromagnetic signals in common diamagnetic oxide crystals, Phys. Rev. B **81**, 214414 (2010).
[55] K. Potzger, J. Osten, A. A. Levin, A. Shalimov, G. Talut, H. Reuther, S. Arpaci, D. Bürger, H. Schmidt, T. Nestler, and D. C. Meyer, Defect-induced ferromagnetism in crystalline $SrTiO_3$, J. Magn. Magn. Mater. **323**, 1551 (2011).
[56] Boris B. Straumal, Andrei A. Mazilkin, Svetlana G. Protasova, Ata A. Myatiev, Petr B. Straumal, Gisela Schütz, Peter A. van Aken, Eberhard Goering, and Brigitte Baretzky, Magnetization study of nanograined pure and Mn-doped ZnO films: Formation of a ferromagnetic grain-boundary foam, Phys. Rev. B **79**, 205206 (2009).
[57] A. Leonhardt, S. Hampel, C. Müller, I. Mönch, R. Koseva, M. Ritschel, D. Elefant, K. Biedermann, and B. Büchner, Synthesis, properties, and applications of ferromagnetic-filled carbon nanotubes, Chem. Vap. Deposition **12**, 380 (2006).

[58] K. Lipert, S. Bahr, F. Wolny, P. Atkinson, U. Weißker, T. Mühl, O. G. Schmidt, B. Büchner, and R. Klingeler, An individual iron nanowire-filled carbon nanotube probed by micro-Hall magnetometry, Appl. Phys. Lett. **97**, 212503 (2010).

[59] T. Mühl, J. Körner, S. Philippi, C. F. Reiche, A. Leonhardt, and B. Büchner, Magnetic force microscopy sensors providing in-plane and perpendicular sensitivity, Appl. Phys. Lett. **101**, 112401 (2012).

[60] J. Nagel, A. Buchter, F. Xue, O. F. Kieler, T. Weimann, J. Kohlmann, A. B. Zorin, D. Rüffer, E. Russo-Averchi, R. Huber, P. Berberich, A. Fontcubertai Morral, D. Grundler, R. Kleiner, D. Koelle, M. Poggio, and M. Kemmler, Nanoscale multifunctional sensor formed by a Ni nanotube and a scanning Nb nanoSQUID, Phys. Rev. B **88**, 064425 (2013).

[61] M. Khapaev, M. Kupriyanov, E. Goldobin, and M. Siegel, Current distribution simulation for superconducting multilayered structures, Supercond. Sci. Technol. **16**, 24 (2003).

[62] Manfred E. Schabes, Micromagnetic theory of non-uniform magnetization processes in magnetic recording particles, J. Magn. Magn. Mater. **95**, 249 (1991).

[63] A. Aharoni, Magnetization curling, Phys. Status Solidi **16**, 3 (1966).

[64] R. Skomski, *Simple Models of Magnetism* (Oxford University Press, New York, 2008).

[65] Amikam Aharoni, Angular dependence of nucleation by curling in a prolate spheroid, J. Appl. Phys. **82**, 1281 (1997).